Journal of Hydrology 584 (2020) 124754

Contents lists available at ScienceDirect

Journal of Hydrology

journal homepage: www.elsevier.com/locate/jhydrol

Research papers

Effects of large macropores on soil evaporation in salt marshes

Tingzhang Zhou[a,b], Pei Xin[a,*], Ling Li[c], D.A. Barry[d], Jirka Šimůnek[b]

[a] State Key Laboratory of Hydrology-Water Resources and Hydraulic Engineering, Hohai University, Nanjing, China
[b] Department of Environmental Sciences, University of California Riverside, Riverside, USA
[c] School of Engineering, Westlake University, Hangzhou, China
[d] Laboratoire de technologie écologique (ECOL), Institut d'ingénierie de l'environnement (IIE), Faculté de l'environnement naturel, architectural et construit (ENAC), Ecole Polytechnique Fédérale de Lausanne (EPFL), Lausanne, Switzerland

ARTICLE INFO

This manuscript was handled by P. Kitanidis, Editor-in-Chief, with the assistance of Martin Thullner, Associate Editor

Keywords:
Salt marsh
Soil evaporation
Macropores
Preferential flow
HYDRUS

ABSTRACT

The occurrence of macropores in salt marsh sediments is a natural and ubiquitous phenomenon. Although they are widely assumed to affect pore-water flow in salt marshes significantly, the mechanisms involved and their extent are not well understood. We conducted laboratory experiments and numerical simulations to examine the effect of macropores on soil evaporation. Soil columns packed with either sand or clay and with or without macropores were set up with watertables in the columns set at different levels. A high potential evaporation rate was induced by infrared light and a fan. The results showed that in the soil with a low saturated hydraulic conductivity (and thus a low water transport capacity), the macropore behaved as a preferential flow path for groundwater to recharge the surrounding soil during evaporation. The evaporated water originated largely from the macropore rather than the soil matrix, maintaining a high evaporation rate in comparison with a homogeneous soil. This effect was more pronounced for sediments with lower hydraulic conductivities and shallower watertables. These results improve our understanding of water flow and evaporation in salt marshes with continuous macropores between the soil surface and groundwater.

1. Introduction

Salt marshes, a type of wetland with herbaceous vegetation (Fig. 1a), are found globally along shorelines (Pendleton et al., 2012). As one of the most productive ecosystems, salt marshes maintain coastal biodiversity and serve as essential habitats for many species of intertidal fauna and flora (Adams, 1963; Moffett et al., 2012; Morris, 1995; Wiegert and Freeman, 1990). They also play essential roles in shoreline protection, fishery support, water quality improvement and carbon sequestration (Pendleton et al., 2012). However, almost half of global salt marshes were lost in the last century (Kennish, 2001), mainly due to land reclamation and sea-level rise (Fagherazzi et al., 2012; Woodworth, 2010). Furthermore, existing marshes are threatened by severe degradation (Balke et al., 2016). Therefore, understanding the behavior of salt marshes subjected to various forcing factors is vital for protecting coastal eco-environments.

Salt marshes are commonly found in the upper part of intertidal zones. Tidal creeks provide pathways for water, solute and energy transport (Wilson and Gardner, 2006; Xin et al., 2011). The amounts of water and solute (e.g., salt) in a creek-marsh system are affected by tides, evapotranspiration (including evaporation and plant root uptake) and rainfall (Moffett et al., 2012; Morris, 1995; Xin et al., 2011, 2017) (Fig. 1a). Water exchange among surface water, groundwater, and the atmosphere affect soil conditions (e.g., soil aeration) and solute transport (e.g., salt accumulation) in salt marshes (Xin et al., 2017). Understanding this exchange is crucial to answering two important scientific questions related to marsh ecology: plant zonation (i.e., plant distribution in an organized fashion with distinct spatial patterns) and nutrient outwelling (i.e., marshes export nutrients to coastal water) (Chapman, 1960; Teal, 1962).

Recently, intensive studies were conducted to examine surface water and groundwater interactions in creek-marsh systems subjected to tides (Adams, 1963; Cao et al., 2012; Moffett et al., 2012; Shen et al., 2018; Ursino et al., 2004; Wilson and Gardner, 2006; Xiao et al., 2017; Xin et al., 2013). They demonstrated a near-creek pore-water circulation, in which water infiltrates from the marsh platform during flood tides and seeps out of the creek bank and bottom during ebb tides (Cao et al., 2012; Wilson and Gardner, 2006; Xin et al., 2011). This circulation affects solute exchange between the marsh and adjacent sea and regulates soil conditions that determine plant growth and marsh functions (Adams, 1963; Colmer and Flowers, 2008; Dacey and Howes, 1984; Marani et al., 2006; Mendelssohn et al., 1981; Wilson et al., 2015;

* Corresponding author.
E-mail address: pei.xin@outlook.com (P. Xin).

https://doi.org/10.1016/j.jhydrol.2020.124754
Received 4 December 2019; Received in revised form 13 February 2020; Accepted 21 February 2020
Available online 24 February 2020

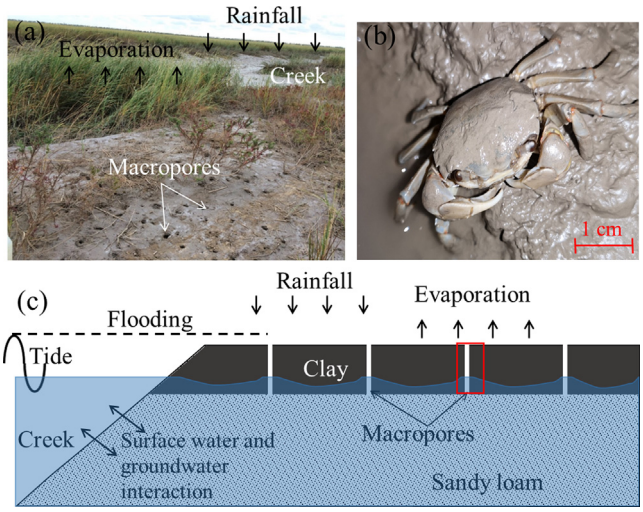

Fig. 1. (a) A photograph of a creek in Chuandong, Jiangsu, China; (b) a photo of a crab; and (c) a schematic diagram of the creek-marsh system with macropores (a red rectangle indicates the system used in this study).

Xin et al., 2013).

By contrast, the effects of evapotranspiration on salt marshes are rarely studied and poorly understood (Xin et al., 2017). Evapotranspiration is a vital component of the global hydrologic cycle and affects the water balance in various hydrological systems (Brutsaert, 1982). Almost 60% of the terrestrial precipitation returns to the atmosphere through evapotranspiration (Oki and Kanae, 2006). Around 25% of the total solar radiation on earth is consumed by evapotranspiration (Or et al., 2013; Trenberth et al., 2009). In salt marshes, evapotranspiration affects pore-water flow and solute transport (Xin et al., 2017). For example, evapotranspiration takes freshwater away but leaves salt behind, resulting in salt accumulation in the shallow soil layer and plant rhizosphere that may inhibit plant growth (Adams, 1963; Morris, 1995; Shen et al., 2018). As evapotranspiration desaturates the soil pores during the marsh emergence, it could increase the water infiltration during the tidal overtopping, resulting in enhanced water and solute exchange between marsh sediment and surface water (Shen et al., 2018).

While understanding of soil evaporation at various scales and in different hydrological systems is well established, previous studies predominately focused on homogeneous soils (Brutsaert, 1982; Haghighi et al., 2013; Or et al., 2013; Penman, 1948). The effects of soil heterogeneity on evaporation are still poorly understood. Heterogeneity can cause major differences in the duration of evaporation stages and total evaporation flux. Lehmann and Or (2009) examined evaporation in heterogeneous soil consisting of coarse and fine sands and found that capillarity drives the liquid from the coarse domain to the fine one and supplies evaporation from fine sand. This prolongs the period of the high evaporation stage, which may increase the total evaporative flux. Assouline and Narkis (2017) found that different irregular soil configurations could cause a shift in the development of the evaporation front and the duration of different evaporation stages.

It is unclear how to transfer existing knowledge of evaporation to highly heterogeneous marsh sediments, which often include macropores such as crab burrows (Fig. 1a, b). For example, fiddler crabs (a species of marine crabs that makes large continuous openings in sediments) are found in a large portion of the global coastline (their global distribution is given in Fig. S1, S refers to Supplementary Materials). Their burrows are known to increase the sediment-water-atmosphere interface and thus affect water flow in salt marshes. Xin et al. (2009) and Xiao et al. (2019) found that macropores behave as preferential pathways and increase the volume of tidally-driven water exchange between marsh soil and tidal creek. Macropores can also improve soil aeration and enhance salt transport in salt marshes, which may favor plant growth (Colmer and Flowers, 2008; Marani et al., 2006; Mendelssohn et al., 1981).

This study is motivated by a field study on a salt marsh in the Yancheng coast (32°43′−34°28′ N, 119°48′−121°15′ E), Jiangsu Province, China. As the typical marsh soil stratigraphy (Carol et al., 2011; Dolphin et al., 1995; Gardner and Porter, 2001; Harvey et al., 1987; Hughes et al., 1998; Perillo et al., 2005; Xin et al., 2009), this site's marsh sediment consists of a low-permeability clay layer overlying a high-permeability sandy-loam layer. The lower sandy-loam layer is relatively well-connected to the creek nearby, and the water-table is controlled by the creek water level. Through the highly-conducted sandy loam layer, the position of the water level in the creek is transferred to the bottom of the clay layer. In this study, we focus only on the surface clay layer and assume that macropores are continuous openings connecting the soil surface with the groundwater from the lower layer. We further assume that evaporation directly from macropores can be neglected and that macropores enhance evaporation across the soil surface by facilitating underground flow towards the surface soil (Fig. 1c).

Based on these assumptions, we conducted laboratory experiments and numerical simulations (in which the vapor flux from the macropore is neglected) on soil evaporation with and without macropores. To expand the results beyond laboratory conditions, a sensitivity analysis with different potential evaporation rates (1, 2, and 3 cm/d) and soil textures (clay, silt loam, and sandy loam) was conducted. The results address the following questions: (1) How do macropores affect soil evaporation rate, water flow, and soil saturation distribution; (2) How are these effects altered by potential evaporation, and (3) How is the soil evaporation affected by macropores in combination with soil properties (hydraulic conductivity and soil water retention curve).

2. Methodology

2.1. Laboratory experiment

Experiments were conducted in two cylindrical soil columns with a height of 75 cm and an inner diameter of 30 cm (Fig. 2a, b). The first column was packed with soil without a macropore. In the second column, a tube of the same length of the column was inserted in the center of the column to act as a macropore (Fig. 2c, d). The tube used in this experiment was made from a metal frame (diameter 4 cm) covered with a stainless mesh (aperture of around 0.1 mm). At the bottom of the columns, permeable porous stones were placed, and the columns were linked to Marriott bottles, which can provide fixed watertables. Both soil columns and Marriott bottles were placed on high-resolution, self-logging scales so that the soil evaporation rates could be determined by weight changes.

Eight sets of experiments with different watertables in the soil column were conducted. The watertables were located between 0 and 70 cm (in a 10-cm interval) below the soil surface. Before each experiment, the top in the Marriott bottles was adjusted, and the bottles were connected with soil columns. At the beginning of each set of experiments, we adjusted the watertables in the Marriott bottle and left the columns to evaporate. Evaporation was considered to reach a steady-state when the weight of the soil column became steady. The columns were then left to evaporate for around additional 10 h and the evaporation rates were calculated as the averaged weight loss of the Marriott bottles.

All the experiments were conducted under well-controlled indoor conditions. An air conditioner was used to maintain a stable temperature and humidity. To shorten the period needed to reach steady-state conditions, we set a high potential evaporation rate. The room temperature and humidity were set to 30 °C and 40%, respectively. For each experimental column, an identical fan was used to generate a steady airflow (around 3.8 m/s), with a channel installed on the top of

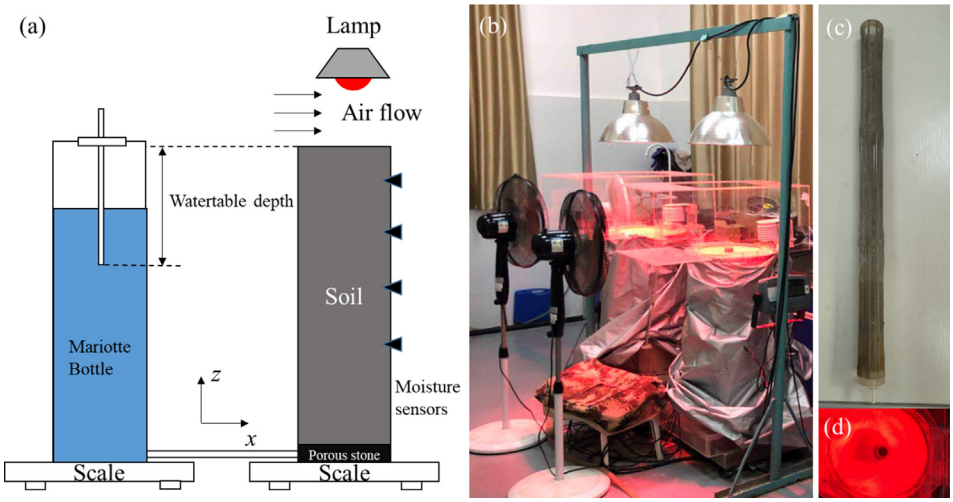

Fig. 2. (a) A schematic diagram of the experimental setup; (b) a photograph of the experimental setup; (c) the tube used as a macropore in the experiments; (d) a photograph of the top of the column with a macropore illuminated by a lamp.

each column to keep airflow uniform. Above the soil columns, infrared lamps (250 W, Philips) were installed for supplying heat to the soil surface. Temperature and relative humidity close to the soil surface and 12 cm above the soil surface were monitored by relative humidity sensors (VP-4, Decagon), which were connected to data loggers. These measured atmospheric conditions were used for calculating the potential evaporation rate (details in Supplementary Materials). Dielectric soil moisture sensors (5TM, Decagon) were installed at 10, 25, 40, and 55 cm below the soil surface to measure the liquid water saturation. The moisture sensors were installed from outside of the soil column, with their tips 5 cm away from the column center.

2.2. Numerical model

To generalize the results from the experiments and obtain further insights into water flow and soil water saturation distributions, we also conducted numerical simulations using HYDRUS (2D/3D) (Šimůnek et al., 2011; Šimůnek et al., 2016). All simulations continued until steady conditions were reached (defined as when the evaporation rate became constant). The soil hydraulic parameters of all materials used in this study are listed in Table 1. The soil water retention curves were measured in the laboratory and then fitted using the van Genuchten (1980) model (Supplementary Materials and Fig. S2).

In this study, the 2D axisymmetric soil domains were discretized using unstructured triangular finite element meshes in an axisymmetric coordinate system (Fig. S3). Although flow in columns without a macropore is expected to be one-dimensional, in order to compare the results from the columns with and without a macropore, we used the same 2D model and the same radially-symmetric coordinate system to simulate flow in the both columns. In all simulations, the wall side boundary was set to no flow. The pressure head was specified at the bottom of the soil column to represent the watertable. For the cases with a macropore, the part of the macropore below the watertable was treated as a fixed-head boundary and the part above the watertable as a no-flow boundary. Since the cross-section of the macropore was quite small in comparison with the soil surface, the evaporation loss from the macropore was neglected in the model.

Table 1
Soil hydraulic parameters (van Genuchten, 1980) for soils used in this study. The first two soil types, i.e., Sand and Clay, were used in the laboratory experimental columns, while the last three soil types, i.e., Sandy Loam, Silt Loam, and Clay-S, were used in the sensitivity analysis.

Soil type	Sand	Clay	Sandy loam	Silt loam	Clay-S
K_s (cm/d)	330.0	1.0	106.1	10.8	4.8
Porosity	0.40	0.38	0.41	0.45	0.38
S_{wres}	0.15	0.18	0.16	0.15	0.18
α (m^{-1})	5	0.27	7.5	2	0.8
n	1.7	1.93	1.89	1.41	1.09

At the soil surface, an atmospheric boundary condition was used to simulate evaporation from the soil. It is well known that actual soil evaporation is determined by the atmospheric condition as well as the soil moisture condition in the surface soil layer (Brutsaert, 1982; Camillo, 1986; van de Griend and Owe, 1994). The former is also termed as potential evaporation and was calculated using a widely used evaporation model based on the measured vapor pressure difference and an aerodynamic resistance during the experiments under steady-state conditions (Figs. S5 and S6) assuming thermodynamic equilibrium between the liquid and gaseous phases (detailed calculations in Supplementary Materials). With potential evaporation (ET_0) determined, soil evaporation (i.e., actual evaporation, EP) was calculated in HYDRUS by limiting the evaporative flux using the following two conditions:

$$EP = -K(h)\left(\frac{\partial h}{\partial z} + 1\right) \leqslant ET_0 \tag{1}$$

$$h_a \leqslant h \leqslant 0 \tag{2}$$

where $K(h)$ is the hydraulic conductivity [LT^{-1}] and h_a is the limiting pressure head (cm) when the first, optimal evaporation stage stops. Note that h_a is a function of the equilibrium between the soil moisture and the atmospheric water vapor, which can be derived using (De Vries, 1958; Philip and De Vries, 1957):

$$h_a = -\frac{RT}{Mg}\ln(H_r) \tag{3}$$

where R is the universal gas constant (8.31 J mol^{-1} K^{-1}), g is the magnitude of gravitational acceleration (9.8 m s^{-2}), M is the molecular weight of water (18 g mol^{-1}), T is the absolute air temperature (°K), and H_r is the relative humidity (set to 40% as maintained by the air conditioner during the experiments).

To shorten the experimental period, we adopted a potential evaporation rate higher than those in natural systems. To generalize the results and get a better insight into real systems, a sensitivity analysis for different potential evaporation rates, i.e., 1, 2, and 3 cm/d (Marani et al., 2006), and different soil textures was conducted. Clay, silt loam, and sandy loam, i.e., three commonly found soil types in salt marshes, were examined in this sensitivity analysis (Table 1 and Fig. S4).

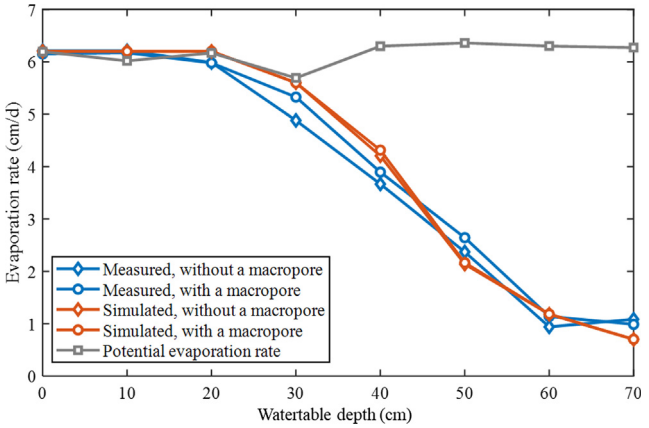

Fig. 3. Measured and simulated (steady state) evaporation rates for the sandy experimental columns with different watertable depths.

3. Results

3.1. Results for the sandy columns

Measured and simulated evaporation rates for the sandy experimental columns with and without a macropore are shown in Fig. 3. In general, evaporation rates can be divided into three groups depending on the position of watertable:

(1) When watertable depths (distance from the watertable to the soil surface) were 0, 10, and 20 cm below the soil surface, the evaporation rates in both columns were largely similar and close to the potential evaporation rate (around 6.2 cm/d). The simulation results were consistent with the experimental results. In addition, the presence of the macropore had no apparent effect on the evaporation rate.
(2) When watertable depths were 30, 40, and 50 cm below the soil surface, the evaporation rates decreased below the potential evaporation rate as the watertable decreased, and correspondingly, the soil became less saturated. Differences in evaporation rates between the two cases (with/without a macropore) were minor, and there were no differences in the simulation results.
(3) When watertable depths were 60 and 70 cm below the soil surface, the evaporation rates were around 1 cm/d. As the watertable declined to this depth, a dry soil layer with low water saturation was detected during the experiment. Evaporation was expected to occur mainly at low rates via water vapor diffusing through the dry soil layer. Note that vapor diffusion was not considered in the numerical simulations.

The saturation profiles in the sand columns are shown in Fig. 4. The measured results show little differences for different watertable depths between 40 and 60 cm, while the lines representing the simulated results overlap. Due to the uncertainty in the experiments, the porosities of the soil columns were not uniform. While the porosity was assumed to be uniform in the numerical simulations, it was likely not uniform in the laboratory soil column experiments due to packing. This non-uniformity may have resulted in differences between the simulated and measured results. According to the simulation, the macropore did not affect saturation distributions in the sand columns, which was consistent with the evaporation rate results. The soil higher than the watertable remained saturated, and the soil profile became drier when the position was closer to the surface. For different watertable depths, the saturation at the soil surface decreased as the watertable was lowered until the watertable reached 40 cm, when the surface saturation was almost equal to the residual saturation.

Based on the simulation results, we examined the distributions of

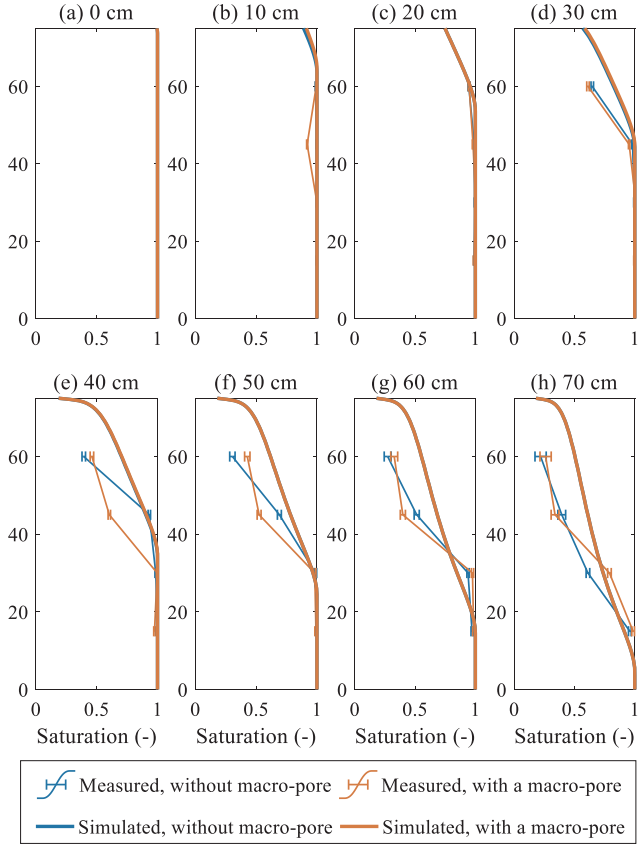

Fig. 4. Measured and simulated saturations for the sandy experimental columns with different watertable depths: (a) 0 cm, (b) 10 cm, (c) 20 cm, (d) 30 cm, (e) 40 cm, (f) 50 cm, (g) 60 cm, and (h) 70 cm). Red lines overlap blue lines. The stand variances of the measured results were given by the horizontal bars.

Darcy flux and soil saturation for different watertable depths (Fig. 5, note the central section across the macropore is shown). The evaporation rates and the saturation distributions were similar in both columns. Above the watertable, saturations decreased with increasing elevation, as expected. However, differences in water fluxes between the two columns were apparent. While the Darcy velocities were uniformly vertical both below and above the watertable in cases without a macropore, horizontal flow occurred below the watertable and around the macropore in cases with a macropore. This was more significant around the watertable, where the Darcy flux was the highest. Clearly, the macropore behaved as a preferential flow path for groundwater to recharge the surrounding soil during evaporation, in which case the evaporated water originated from the macropore rather than the soil matrix.

We further calculated horizontal fluxes from the macropore to the soil (Fig. 6). Consistent with the flow field discussed earlier, the horizontal flux varied with elevation and the position of the watertable. With the watertable at the soil surface, horizontal fluxes started from 0 cm/d and increased monotonically as the elevation increased. In contrast, for deeper watertables, the horizontal flux increased first and then decreased around the watertable. For the cases with a macropore, the evaporative flux originates both from water in the macropore (called macropore water) and water flowing upwards from the base of the column through the soil profile. We calculated the ratios between fluxes through the macropore and actual evaporation fluxes (Table 2). The ratios were very high (over 90%) when watertable depths were less than 40 cm. The ratios dropped rapidly for deeper watertables, e.g., from 79.7% for a 50-cm depth to 18.1% for a 70-cm depth, i.e., the effect of the macropore on soil evaporation was more critical for the soil with shallow watertables.

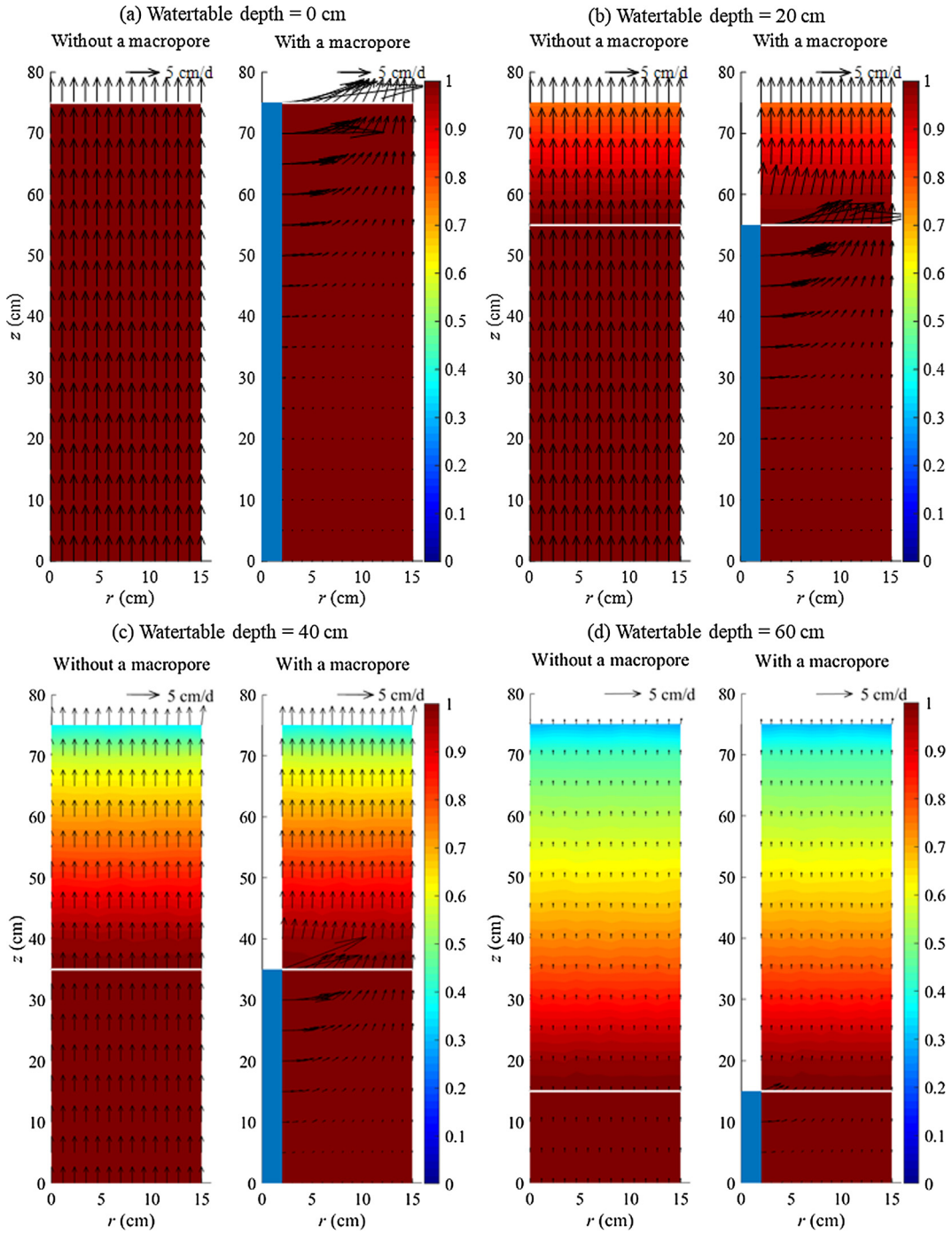

Fig. 5. Simulation results for the sandy experimental columns without (left) and with (right) a macropore for watertable depths of (a) 0 cm, (b) 20 cm, (c) 40 cm, and (d) 60 cm. Water saturation is shown in color, while the arrows represent the Darcy velocities (the magnitude is indicated by the arrow length). The white lines indicate the position where the hydraulic head is equal to 0.

3.2. Results for the clay columns

The results for the experiments with clay were more complex than those for sand. The particle size distribution for clay was wider (d_{90}/d_{10} = 12.96), suggesting a wider distribution of pore sizes. Soil heterogeneity might have increased due to the experimental setup, as it was difficult to control the soil packing. Indeed, in order to satisfactorily simulate the measured results for columns with clay soil without a macropore, the saturated hydraulic conductivity was set to 1.0 cm/d and the van Genuchten parameters α and n to 0.27 m^{-1} and 1.93, respectively (Table 1). However, these values failed to describe the experimental data for clay columns with a macropore, due to uncertainty caused by soil packing (Fig. 7). The numerical model described the experimental data satisfactorily only with manually adjusted parameter values (i.e., the saturated hydraulic conductivity of 1.9 cm/d and the van Genuchten parameters α = 0.27 m^{-1} and n = 2.23).

In the clay columns without a macropore, different watertable depths did not produce different evaporation rates, as in the sand columns. In the clay columns, the evaporation rates were low and changed only slightly for different watertable levels. Since the potential evaporation rate was much higher than the permeability of the soil, the low

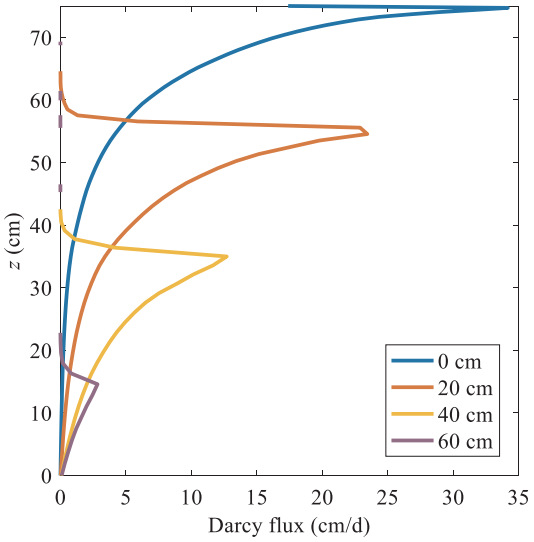

Fig. 6. Simulated horizontal Darcy fluxes at the macropore boundary of the sandy columns with different watertable depths.

Table 2
Ratios (in %) of the water flux through the macropore to the actual evaporation rate in experimental columns with different watertable depths and soil types.

Soil Type	Watertable depth (cm)							
	0	10	20	30	40	50	60	70
Sand	99.3	98.9	98.1	95.8	90.5	79.7	53.0	18.1
Clay	99.3	99.2	98.1	96.0	90.5	80.8	59.3	20.0

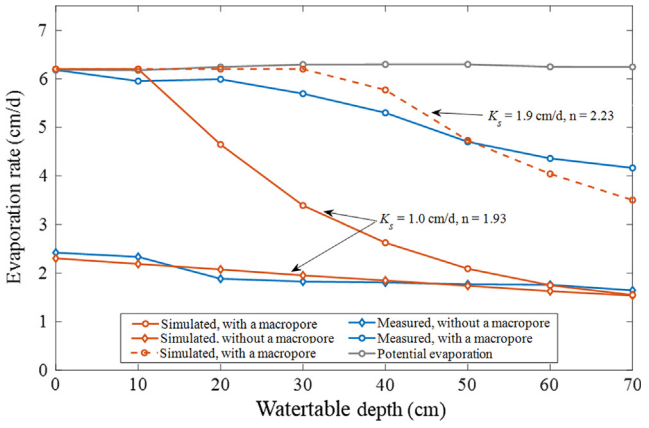

Fig. 7. Measured and simulated steady state evaporation rates for the clay experimental columns with different watertable depths. The solid red lines represent simulation with the same soil properties, with and without a macropore. The dashed red line represents the simulation using the adjusted soil properties (K_s = 1.9 cm/d, n = 2.23) that fit well the experimental results.

hydraulic conductivity of the clay prevented actual evaporation from reaching the potential evaporation even for shallow watertables (0 and 20 cm). Also, the zero-pressure head line in the soil (i.e., depth where the pressure head was equal to zero) was significantly lower than the corresponding applied pressure head at the bottom of the column. In contrast, two different evaporation scenarios were observed for the cases with a macropore. Evaporation rates were almost constant and close to the potential evaporation rate when the watertable was close to the soil surface (0 and 10 cm). After the watertable dropped to 20 cm, evaporation rates decreased and continued to do so as the watertable was lowered further.

Interestingly, actual evaporation for the watertable depth of 70 cm was 1.7 cm/d, higher than that for the sand case (when it was less than 1 cm/d). At this level, the watertable was close to the soil column bottom, and thus the impact of the macropore was minor. Instead, it was the large capillary fringe of the clay and higher unsaturated hydraulic conductivity that led to the higher evaporation rate.

For the clay columns, the distributions of Darcy fluxes and soil saturations for different watertable levels differed significantly for scenarios without and with a macropore (Fig. 8, note the central section across the macropore is shown). For the former, the one-dimensional behavior is again apparent, similar to the sand cases. The fluxes were uniform and vertical. The soil saturation decreased with increasing elevation in the unsaturated zone. In the near-surface area, neither fluxes nor soil saturations were significantly affected by the watertable depth. However, the two-dimensional behavior occurred around the macropore. Overall, the watertable (defined as the zero-pressure head line) decreased from the macropore to the soil-wall boundary. Accordingly, the local soil water saturation decreased, as shown in Fig. 8a. When the watertable in the macropore was close to the soil surface, the area far away from the macropore was unsaturated. As the watertable depth increased from 0 to 20, 40, and 60 cm, the flux in the near-soil surface area decreased, which is consistent with the reduced evaporation rates. In this area, the soil saturation was also reduced as the watertable was lowered.

Overall trends and variations in the simulated horizontal fluxes through the macropore boundary for the clay columns were similar to those for the sandy columns (compare Fig. 9 with Fig. 6). Fluxes similarly decreased with the lower groundwater level and reached their peaks around the watertable. Like the sand cases, the ratio of water flowing from the macropore to the actual evaporation rate was significant (more than 90%) when the watertable depths were less than 40 cm. It then dropped from around 80% for a 50-cm depth to 19.9% for a 70-cm depth. These ratios for the clay cases were slightly higher than those for the sand cases (Table 2).

3.3. Sensitivity analysis to potential evaporation

Overall, trends and variations of actual evaporation rates were consistent with experimental evaporation rates for the sand case, i.e., shallow watertables led to high evaporation rates. The effects of a macropore on evaporation rates were more pronounced for soils with a lower hydraulic conductivity, i.e., clay and silt loam. For sandy loam, no apparent differences were caused by a macropore, and evaporation rates for columns with and without a macropore overlapped (Fig. 10).

For silt loam, evaporation rates for columns with a macropore were larger than for columns without a macropore for the same positions of water tables, e.g., for a watertable depth at 40 cm and ET_0 of 1 cm/d (Fig. 10). The macropore effect increased as the potential evaporation rate increased. For ET_0 = 3 cm/d, evaporation rates for columns with a macropore were larger than those for columns without a macropore for watertable depths from 10 to 50 cm. As the potential evaporation rate increased, the macropore played an increasingly important role in affecting the actual evaporation rates for cases with shallow watertables.

For both silt loam and sandy loam, actual evaporation rates for scenarios without a macropore reached the potential evaporation rate when the watertable was close to the soil surface, indicating that soils were permeable and able to maintain a high evaporation rate. In contrast, clay, with the lowest hydraulic conductivity among all three soil types, could not support a high evaporation rate without a macropore. This result was demonstrated by the results with shallow watertables. For a watertable close to the soil surface, evaporation rates were similar for scenarios with and without a macropore for ET_0 = 1 cm/d. As ET_0 increased to 2 and 3 cm/d, scenarios with a macropore still reached the potential evaporation rate, but for those without a macropore, actual evaporation rates decreased to around 1 cm/d, which was the value of the soil saturated hydraulic conductivity.

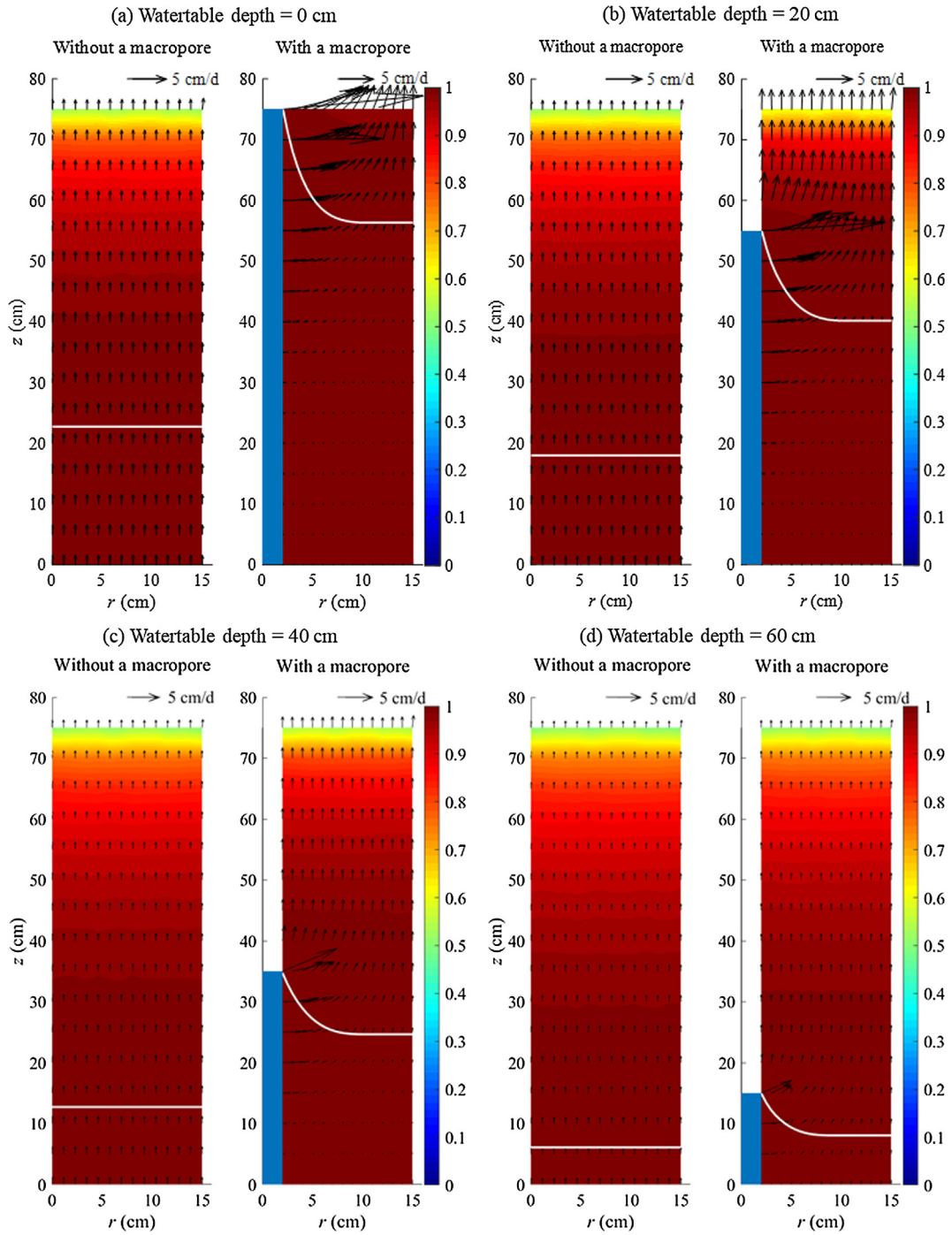

Fig. 8. Simulation results for the clay experimental columns without (left) and with (right) a macropore for watertable depths of (a) 0 cm, (b) 20 cm, (c) 40 cm, and (d) 60 cm. The saturation is shown in color, while the arrows represent the Darcy velocities (the magnitude is indicated by the arrow length). White lines indicate the position where the hydraulic head is equal to 0.

Ratios of water fluxes through the macropore to the actual evaporation rate for cases considered in the sensitivity analysis are demonstrated in Fig. 11. Overall trends and values for these cases are similar to the experimental cases, being over 90% when the watertable depths are less than 40 cm and dropping rapidly from 80.7% for a 50-cm watertable depth to about 20% for a 70-cm watertable depth. Different potential evaporation rates and soil properties did not show much influence on the ratios of water fluxes from a macropore to the actual evaporation rate. These results indicate that the watertable depth significantly affects the water bypass caused by the macropore.

4. Discussion

While this study focused on water flow in cylindrical soil columns, it should help to increase our understanding of the effects of macropores on water flow and solute transport in real salt marshes. Macropores did not affect soil evaporation markedly in high-permeability soils such as sandy loam. However, low-permeability silt loams and clays were unable to deliver enough water to the soil surface to maintain a high evaporation rate. Under such conditions, continuous macropores in contact with groundwater behave as preferential flow paths, providing water for evaporation.

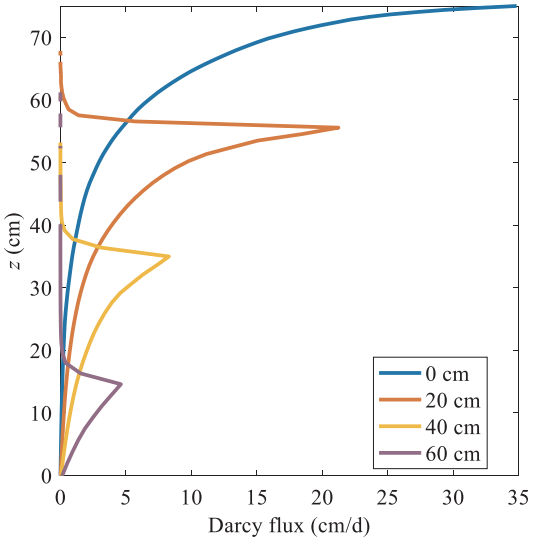

Fig. 9. Simulated horizontal Darcy fluxes at the macropore boundary for the clay columns with different watertable depths.

Soil layering is commonly found in natural marshes: a low-permeability clay layer overlying a high-permeability sandy-loam layer (Cao et al., 2012; Dolphin et al., 1995; Xiao et al., 2017; Xin et al., 2012). Enhanced evaporation would intensify water exchange between creek water and marsh soil. While creek water in natural systems is commonly saline and evaporation would lead to soil salinization (Xin et al., 2017), we used freshwater in this study to minimize this effect.

For soils with shallow watertables, macropores increased soil saturation in shallow soil layers. This is expected to lower soil aeration and oxygen availability in marsh soils, which could affect plant root respiration and thus marsh plant growth (Colmer and Flowers, 2008; Dacey and Howes, 1984; Mendelssohn et al., 1981; Silvestri et al., 2005). However, in macropores, there is no capillary-induced upward flow, which would decrease soil saturation of near-surface soil layers in soils next to macropores with deeper watertables. Under such conditions, evaporation would be reduced, similarly as associated water exchange. Natural marshes are periodically inundated by tidal water. For less saturated soils, tidal infiltration would increase, which would lead to enhanced water exchange in shallow marsh soils.

Our results show that the contribution of water from the macropore to the evaporation flux is significant compared with that which comes from the watertable and passes entirely through the soil before evaporation. With denser distributions of macropores, most of the evaporated water would bypasses the soil matrix and has only a little contact with soil grains. This is expected to affect the fate of chemicals transported through marsh soils. For example, chemicals in deep soil layers would be unlikely to be transported to the shallow soil layers due to weak upward flow. Furthermore, interactions between the deep soil layer and creek water would be weakened.

Guimond et al. (2019) recently found that the presence of macropores reduces carbon sequestration in salt marshes. This is consistent with Xin et al. (2009) and Xiao et al. (2019) who indicated that macropores likely enhance lateral water exchange between marsh soil and creek water, which may increase a lateral loss of dissolved carbon. These same authors also suggested that macropores would decrease soil water saturation of the shallow soil layer and thus improve local soil aeration conditions. This would favor carbon oxidation and lead to a further vertical carbon loss. Our results indicate that while macropores enhance evaporation from soil columns with a fixed watertable, the soil

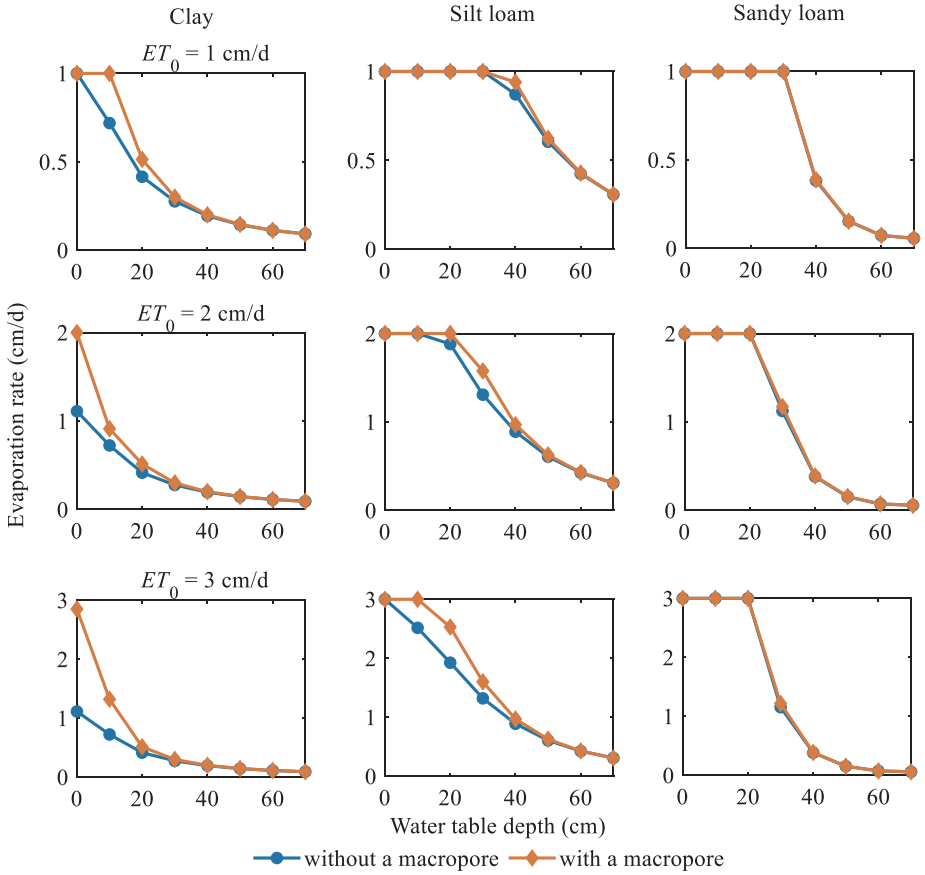

Fig. 10. The effects of potential evaporation (ET_0) and soil type on actual evaporation for soils with and without a macropore. The first, second, and third columns show the simulation results for clay, silt loam, and sandy loam, respectively. The potential evaporation rates are the same for each row and given in the figure titles.

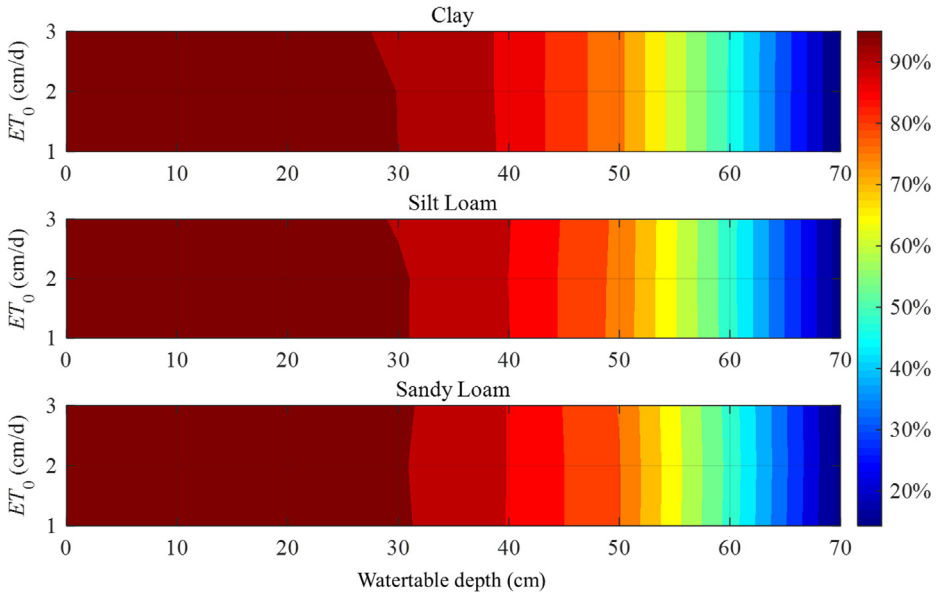

Fig. 11. Ratios (in %) of the water flux through the macropore to the actual evaporation rate for different potential evaporation rates (ET_0 = 1–3 cm/d), groundwater levels (0–70 cm), and soil types (clay, silt loam, and sandy loam) considered in the sensitivity analysis.

water saturation in the upper soil layer is increased. This would lead to reduced oxygen availability and inhibited carbon oxidation. This is inconsistent with previous studies (Xin et al., 2009; Xiao et al., 2019). In natural salt marshes, evaporation would lower a local watertable, which would improve soil aeration of the shallow soil layer. The effects of macropores on carbon sequestration thus depend on how they synergistically regulate lateral water flow, the position of the watertable, and associated aeration conditions.

Natural marshes are affected by the combination of evaporation, rainfall and tidal fluctuations. Watertables are dynamic, particularly in near-creek zones (Wilson and Gardner, 2006; Xin et al., 2011). Our results indicate that when watertables are at different depths, the effects of macropores on soil evaporation are not consistent. Macropores are expected to speed up soil evaporation in the clay marsh with shallow watertables that often occur after tidal inundation or rainfall events. However, the near-surface soil is hard to desaturate as macropores allow water to be easily transported from the lower soil profile. As roots of marsh plants are distributed in the shallow soil layer, this more rapid evaporation would not reduce the period of oxygen deficiency, which would not favor plant growth.

5. Conclusions

Based on laboratory experiments and numerical simulations, we examined the effects of large macropores on soil evaporation in soil columns. From the results, the following conclusions can be drawn:

(1) The macropore increased evaporation rates in low-permeability soils with shallow watertables. The macropore did not significantly affect soil evaporation in high permeability soils (e.g., sand and sandy loam).
(2) The presence of the macropore altered water flow in the soil compared to that without the macropore. The macropore behaved as a preferential flow path, delivering groundwater to the shallow soil, which resulted in higher soil saturation in the near-surface area.
(3) Water flow from the macropore contributed significantly to the actual evaporation rate, and this proportion was reduced as the watertable declined. Vertical flow through the soil profile (i.e., independent of the macropore) was reduced by the presence of a macropore.

While the present study has produced insights into steady-state evaporation in salt marshes, it focused on steady-state conditions in idealized soil columns with steady watertables. Further investigations should be conducted to confirm the results from this study in real marshes, in which tides, rainfall, and evaporation would lead to dynamic watertables. Macropores are distributed randomly and vary in diameter and depth. Furthermore, the density and size of macropores likely vary spatially and are related to creek networks. Notwithstanding these differences, the present study highlights the importance of macropores on soil evaporation, and their potential effects on surface water and groundwater interactions and solute transport/reaction in salt marshes.

CRediT authorship contribution statement

Tingzhang Zhou: Methodology, Formal analysis, Data curation, Writing - original draft. **Pei Xin:** Conceptualization, Writing - review & editing, Supervision. **Ling Li:** Methodology, Formal analysis, Validation. **D.A. Barry:** Methodology, Formal analysis, Validation. **Jirka Šimůnek:** Methodology, Writing - review & editing.

Declaration of Competing Interest

The authors declare that they have no known competing financial interests or personal relationships that could have appeared to influence the work reported in this paper.

Acknowledgment

This work was supported by the National Natural Science Foundation of China (51579077).

Appendix A. Supplementary data

Supplementary data to this article can be found online at https://doi.org/10.1016/j.jhydrol.2020.124754.

References

Adams, D.A., 1963. Factors influencing vascular plant zonation in North Carolina salt marshes. Ecology 44 (3), 445–456. https://doi.org/10.2307/1932523.

Assouline, S., Narkis, K., 2017. Evaporation from soil containers with irregular shapes. Water Resour. Res. 53 (11), 8795–8806. https://doi.org/10.1002/2017wr021166.
Balke, T., Stock, M., Jensen, K., Bouma, T.J., Kleyer, M., 2016. A global analysis of the seaward salt marsh extent: the importance of tidal range. Water Resour. Res. 52 (5), 3775–3786. https://doi.org/10.1002/2015wr018318.
Brutsaert, W., 1982. Evaporation into the Atmosphere: Theory, History, and Applications. Springer Netherlands. doi:10.1007/978-94-01w7-1497-6.
Camillo, P.J., 1986. Resistance parameter for bare-soil evaporation models. Soil Sci. 141, 95–105. https://doi.org/10.1097/00010694-198602000-00001.
Cao, M., Xin, P., Jin, G., Li, L., 2012. A field study on groundwater dynamics in a salt marsh – Chongming Dongtan wetland. Ecol. Eng. 40 (Supplement C), 61–69. https://doi.org/10.1016/j.ecoleng.2011.12.018.
Carol, E.S., Kruse, E.E., Pousa, J.L., 2011. Influence of the geologic and geomorphologic characteristics and of crab burrows on the interrelation between surface water and groundwater in an estuarine coastal wetland. J. Hydrol. 403 (3), 234–241. https://doi.org/10.1016/j.jhydrol.2011.04.007.
Chapman, V.J., 1960. Salt marshes and salt deserts of the world. Ecol. Halophytes 213–214.
Colmer, T.D., Flowers, T.J., 2008. Flooding tolerance in halophytes. New Phytol. 179 (4), 964–974. https://doi.org/10.1111/j.1469-8137.2008.02483.x.
Dacey, J.W.H., Howes, B.L., 1984. Water uptake by roots controls water table movement and sediment oxidation in short spartina marsh. Science 224 (4648), 487–489. https://doi.org/10.1126/science.224.4648.487.
De Vries, D.A., 1958. Simultaneous transfer of heat and moisture in porous media. Eos, Trans. Am. Geophys. Union 39 (5), 909–916. https://doi.org/10.1029/TR039i005p00909.
Dolphin, T.J., Hume, T.M., Parnell, K.E., 1995. Oceanographic processes and sediment mixing on a sand flat in an enclosed sea, Manukau Harbour, New Zealand. Marine Geol. 128 (3–4), 169–181. https://doi.org/10.1016/0025-3227(95)00097-i.
Fagherazzi, S., et al., 2012. Numerical models of salt marsh evolution: ecological, geomorphic, and climatic factors. Rev. Geophys. 50 (1). https://doi.org/10.1029/2011rg000359.
Gardner, L.R., Porter, D.E., 2001. Stratigraphy and geologic history of a southeastern salt marsh basin, North Inlet, South Carolina, USA. Wetlands Ecol. Manage. 9 (5), 371–385. https://doi.org/10.1023/a:1012060408387.
Guimond, J.A., Seyfferth, A.L., Moffett, K.B., Michael, H.A., 2019. A physical-biogeochemical mechanism for negative feedback between marsh crabs and carbon storage. Environ. Res. Lett. https://doi.org/10.1088/1748-9326/ab60e2.
Haghighi, E., Shahraeeni, E., Lehmann, P., Or, D., 2013. Evaporation rates across a convective air boundary layer are dominated by diffusion. Water Resour. Res. 49 (3), 1602–1610. https://doi.org/10.1002/wrcr.20166.
Harvey, J.W., Germann, P.F., Odum, W.E., 1987. Geomorphological control of subsurface hydrology in the creekbank zone of tidal marshes. Estuar. Coast. Shelf Sci. 25 (6), 677–691. https://doi.org/10.1016/0272-7714(87)90015-1.
Hughes, C.E., Binning, P., Willgoose, G.R., 1998. Characterisation of the hydrology of an estuarine wetland. J. Hydrol. 211 (1–4), 34–49. https://doi.org/10.1016/s0022-1694(98)00194-2.
Kennish, M.J., 2001. Coastal salt marsh systems in the US: a review of anthropogenic impacts. J. Coastal Res. 17 (3), 731–748.
Lehmann, P., Or, D., 2009. Evaporation and capillary coupling across vertical textural contrasts in porous media. Phys. Rev. E 80 (4), 046318. https://doi.org/10.1103/PhysRevE.80.046318.
Marani, M., et al., 2006. Spatial organization and ecohydrological interactions in oxygen-limited vegetation ecosystems. Water Resour. Res. 42, W06D06. https://doi.org/10.1029/2005wr004582.
Mendelssohn, I.A., McKee, K.L., Patrick, W.H., 1981. Oxygen deficiency in spartina alterniflora roots: metabolic adaptation to anoxia. Science 214 (4519), 439–441. https://doi.org/10.1126/science.214.4519.439.
Moffett, K.B., Gorelick, S.M., McLaren, R.G., Sudicky, E.A., 2012. Salt marsh ecohydrological zonation due to heterogeneous vegetation-groundwater-surface water interactions. Water Resour. Res. 48, W02516. https://doi.org/10.1029/2011wr010874.
Morris, J.T., 1995. The mass balance of salt and water in intertidal sediments: results from North Inlet, South Carolina. Estuaries 18 (4), 556–567. https://doi.org/10.2307/1352376.
Oki, T., Kanae, S., 2006. Global hydrological cycles and world water resources. Science 313 (5790), 1068–1072. https://doi.org/10.1126/science.1128845.
Or, D., Lehmann, P., Shahraeeni, E., Shokri, N., 2013. Advances in soil evaporation physics—a review. Vadose Zone J. 12, 1–16. https://doi.org/10.2136/vzj2012.0163.
vzj2012.0163.
Pendleton, L., et al., 2012. Estimating global "Blue Carbon" emissions from conversion and degradation of vegetated coastal ecosystems. PLoS ONE 7 (9), 7. https://doi.org/10.1371/journal.pone.0043542.
Penman, H.L., 1948. Natural evaporation from open water, hare soil and grass. Proc. R. Soc. Lond. A 193 (1032), 120–145. https://doi.org/10.1098/rspa.1948.0037.
Perillo, G.M.E., Pérez, D.E., Piccolo, M.C., Palma, E.D., Cuadrado, D.G., 2005. Geomorphologic and physical characteristics of a human impacted estuary: Quequén Grande River Estuary, Argentina. Estuar. Coast. Shelf Sci. 62 (1), 301–312. https://doi.org/10.1016/j.ecss.2004.09.018.
Philip, J.R., De Vries, D.A., 1957. Moisture movement in porous materials under temperature gradients. Eos, Trans. Am. Geophys. Union 38 (2), 222–232. https://doi.org/10.1029/TR038i002p00222.
Shen, C.J., Zhang, C.M., Xin, P., Kong, J., Li, L., 2018. Salt dynamics in coastal marshes: formation of hypersaline zones. Water Resour. Res. 54 (5), 3259–3276. https://doi.org/10.1029/2017wr022021.
Silvestri, S., Defina, A., Marani, M., 2005. Tidal regime, salinity and salt marsh plant zonation. Estuar. Coast. Shelf Sci. 62 (1–2), 119–130. https://doi.org/10.1016/j.eess.2004.08.010.
Šimůnek, J., van Genutchen, M.Th., Šejna, M., 2011. The HYDRUS Software Package for Simulating Two- and Three-Dimensional Movement of Water, Heat, and Multiple Solutes in Variably-Saturated Porous Media, Technical Manual, Version 2.0. PC Progress, Prague, Czech Republic.
Šimůnek, J., van Genuchten, M.T., Šejna, M., 2016. Recent developments and applications of the HYDRUS computer software packages. Vadose Zone J. 15https://doi.org/10.2136/vzj2016.04.0033. vzj2016.04.0033.
Teal, J.M., 1962. Energy flow in the salt marsh ecosystem of Georgia. Ecology 43 (4), 614–624. https://doi.org/10.2307/1933451.
Trenberth, K.E., Fasullo, J.T., Kiehl, J., 2009. Earth's global energy budget. Bull. Am. Meteorol. Soc. 90 (3), 311–324. https://doi.org/10.1175/2008bams2634.1.
Ursino, N., Silvestri, S., Marani, M., 2004. Subsurface flow and vegetation patterns in tidal environments. Water Resour. Res. 40 (5), W05115. https://doi.org/10.1029/2003wr002702.
van de Griend, A.A., Owe, M., 1994. Bare soil surface resistance to evaporation by vapor diffusion under semiarid conditions. Water Resour. Res. 30 (2), 181–188. https://doi.org/10.1029/93WR02747.
van Genuchten, M.Th., 1980. A closed-form equation for predicting the hydraulic conductivity of unsaturated soils. Soil Sci. Soc. Am. J. 44 (5), 892–898. https://doi.org/10.2136/sssaj1980.03615995004400050002x.
Wiegert, R.G., Freeman, B.J., 1990. Tidal salt marshes of the southeast Atlantic Coast: A community profile. United States. doi:10.2172/5032823.
Wilson, A.M., et al., 2015. Groundwater controls ecological zonation of salt marsh macrophytes. Ecology 96 (3), 840–849. https://doi.org/10.1890/13-2183.1.
Wilson, A.M., Gardner, L.R., 2006. Tidally driven groundwater flow and solute exchange in a marsh: numerical simulations. Water Resour. Res. 42, W01405. https://doi.org/10.1029/2005wr004302.
Woodworth, P.L., 2010. A survey of recent changes in the main components of the ocean tide. Cont. Shelf Res. 30 (15), 1680–1691. https://doi.org/10.1016/j.csr.2010.07.002.
Xiao, K., et al., 2017. Tidal groundwater flow and its ecological effects in a brackish marsh at the mouth of a large sub-tropical river. J. Hydrol. 555, 198–212. https://doi.org/10.1016/j.jhydrol.2017.10.025.
Xiao, K., Wilson, A.M., Li, H., Ryan, C., 2019. Crab burrows as preferential flow conduits for groundwater flow and transport in salt marshes: a modeling study. Adv. Water Resour. 132, 103408. https://doi.org/10.1016/j.advwatres.2019.103408.
Xin, P., Jin, G., Li, L., Barry, D.A., 2009. Effects of crab burrows on pore water flows in salt marshes. Adv. Water Resour. 32 (3), 439–449. https://doi.org/10.1016/j.advwatres.2008.12.008.
Xin, P., Kong, J., Li, L., Barry, D.A., 2012. Effects of soil stratigraphy on pore-water flow in a creek-marsh system. J. Hydrol. 475, 175–187. https://doi.org/10.1016/j.jhydrol.2012.09.047.
Xin, P., Li, L., Barry, D.A., 2013. Tidal influence on soil conditions in an intertidal creek-marsh system. Water Resour. Res. 49. https://doi.org/10.1029/2012WR012290.
Xin, P., Yuan, L.-R., Li, L., Barry, D.A., 2011. Tidally driven multiscale pore water flow in a creek-marsh system. Water Resour. Res. 47, W07534. https://doi.org/10.1029/2010wr010110.
Xin, P., et al., 2017. Combined effects of tides, evaporation and rainfall on the soil conditions in an intertidal creek-marsh system. Adv. Water Resour. 103 (2017), 1–15. https://doi.org/10.1016/j.advwatres.2017.02.014.